# 2D-CRS stack: A comparison between the extended and global search strategies

*G. Garabito and W. Paschoal*

**email:** *german@ufpa.br*

**keywords:** *Imaging, Coherency, Optimization*

**ABSTRACT**

*The seismic imaging method called Common-Reflection-Surface (CRS) stack simulates a zero-offset (ZO) section from multi-coverage seismic data. Unlike the conventional time imaging method (NMO/DMO stack), the CRS stack method does not depend on the macro-velocity model. For the 2-D case, the hyperbolic traveltime approximation used by the CRS stack depends on three kinematic attributes, which defines a stacking surface for each sampling point in the ZO section to be simulated. The main task of CRS stack method is the estimation of these three optimal attributes by means of automatic search strategies, based on coherence analysis evaluated in the prestack data. Currently, based on two different parameter search strategies, called extended CRS search strategy and global CRS search strategy, there are two CRS stack implementations, that were validated by simulating ZO sections from synthetic and real data sets. Their results have been compared to other similar results, obtained by the conventional NMO/DMO stack method. In this paper, we present a short description of these two CRS strategies and compare both implementations in their application to the well known Marmousi data set. The comparison reveals that the global CRS search is less fast, but it produces better results than extended CRS search strategy.*

## INTRODUCTION

The sesmic imaging has as its main goal generate the best possible image of subsurface geological structures from seismic reflection data. In the last years, it has been proposed several macro-model-independent imaging methods to simulate ZO sections from 2-D multi-coverage data. These kind of methods are discussed in details in a special issue of the *Journal of Applied Geophysics*, edited by (Hubral, 1999). One of these imaging methods that is becoming an alternative to the conventional time seismic imaging methods, like the NMO/DMO stack, is the so-called Common-Reflection-Surface (CRS) stack, that provides a simulated ZO section from multi-coverage data sets. Successful applications of this method to real data sets are shown in (Mann et al., 1999), (Trappe et al., 2001), (Bergler et al., 2002), (Gierse et al., 2003), (Garabito et al., 2003). The CRS stack provides a ZO section with a high signal-to-noise ratio and a good resolution, and also provides three stacking attribute sections that can be useful for others applications, such as velocity model determination (Biloti et al., 2002), (Duveneck, 2004), and AVO analysis (Pruessmann et al., 2004).

In the 2-D case, the CRS stacking surface, also referred as CRS stacking operator, is defined by the hyperbolic traveltime approximation for rays in the vicinity of the ZO central ray. This traveltime approximation depends on three kinematic attributes: the emergency angle $\beta_0$ of the ZO central ray, and the curvatures $K_{NIP}$ and $K_N$ of two hypothetical wavefronts called Normal-Incidence-Point (NIP) wave and Normal (N) wave, respectively Hubral (1983). The hyperbolic traveltime, here called as CRS traveltime approximation, is a second-order Taylor expansion of the reflection traveltime for paraxial rays in the vicinity of a normal incident ray, and can be derived by means of the paraxial ray theory ((Schleicher et al., 1993); (Tygel et al., 1997)) or by a geometrical approach (Höcht et al., 1999). These tree kinematic attributes

of traveltime approximation define the CRS stacking surface in the midpoint-offset-time coordinates. For homogeneous models, the CRS stacking surface is an approximation of the kinematic multi-coverage reflection response of a curved reflector segment in the subsurface. Then, these three stacking parameters supply informations of the reflector segment orientation, its location and its curvature. For heterogeneous models, these stacking attributes can still be used to define the stacking operator, assuming that the emerging hypothetical wavefronts to be circular in a certain vicinity of the emerging point of the central ray. Therefore, assuming that the near-surface velocity is constant, the CRS stack method can be applied to complex media with arbitrary vertical and lateral heterogeneities.

One of the main tasks for the implementation of the CRS stack method consists in the determination of three optimal CRS attributes or CRS parameters from multi-coverage data. These stacking parameters can be estimated using automatic search strategies, based on coherence measure (e.g., semblance), evaluated along the CRS stacking surface in the prestack data. The reader may found details about these CRS strategies in Müller (1998), (Birgin et al., 1999), (Jäger et al., 2001), Mann (2001) and (Garabito et al., 2001). In this paper we are interested in the well estlabished two CRS stack implementations that use different parameters search strategies. The first is the so called *extended CRS search strategy* developed by Mann (2001), and the second is the so called *global CRS search strategy*, developed by (Garabito et al., 2001). The CRS stack implementations based on these two CRS search strategies were initially validated to simulate ZO sections and to determine the kinematic wavefield attributes from synthetic multi-coverage data sets corresponding to simple layered models, with homogeneous layers separated by curved interfaces. Afterwards, these two CRS stack implementations were applied with successful results to real land and marine data sets, and their respective results had been compared with the results of the conventional NMO/DMO stack and other imaging methods, such as post- and pre-stack migrations ((Trappe et al., 2001), (Bergler et al., 2002), (Gierse et al., 2003)).

The *extended CRS search strategy* in its initial phase consists of three one-parametric search steps to determine the initial three stacking parameters for each ZO sample. In this strategy, to handle properly the conflicting dipping events for each ZO sample, additional one-parametric searches are performed. This provides a set of three kinematic attributes for each of the conflicting events. In the final refinement step, using as initial approximation the three parameters determined in the previous one-parametric searches, it is performed a three-parametric local search by applying the (Nelder and Mead, 1965) flexible polyhedron optimization algorithm.

The *global CRS search strategy* consists of three main steps to determine the CRS parameters. In the firts two steps, three initial parameters are determined by applying a two-parametric search and a one-parametric search using the global optimization algorithm Simulated Annealing (SA) (Kirkpatrick et al., 1983). Similar to the first CRS strategy, the third step refines the previously estimated parameters using the Quasi-Newton (QN) local optimization algorithm (Gill et al., 1981). To take in account the conflicting dipping events, this strategy considers, in addition to the global maximum, one local maximum.

In this paper we present a comparison of these two 2D-CRS stack implementations, i.e., the extended CRS search strategy and the global CRS search strategy. Here we only present a brief review of these two different CRS parameter search strategies, since a detailed descripion of them can be found in (Jäger et al., 2001), Mann (2001) and (Garabito et al., 2001). To evaluate the robustness of both CRS stack implementations in order to simulate ZO sections corresponding to complex geological areas, we apply the referred strategies in the imaging of the Marmousi data set.

## CRS TRAVELTIME APPROXIMATION

The CRS traveltime approximation defines a *stacking surface*, where it approximates the reflection traveltime for finite-offset rays in the vicinity of a normal incidence ray, the so-called central ray. The emergence point on the seismic line and the two-way traveltime of the ZO central ray are denoted by $x_0$ and $t_0$, respectively. The CRS traveltime approximation is a hyperbolic second-order Taylor expansion expressed as function of three independent wavefront attributes of the hypothetical Normal-Incident-Point (NIP) and Normal waves, both related to the central ray (Hubral, 1983). These attributes are: the emergence angle $\beta_0$ of the ZO central ray, the radius of curvature $R_{NIP} = \frac{1}{K_{NIP}}$ of the NIP wave and the radius of curvature $R_N = \frac{1}{K_N}$ of the Normal wave. The NIP wave is an upgoing wave that originates at the normal incidence point of the central ray on the reflector. The Normal wave is an exploding reflector wave, with an initial

wavefront curvature equal to the local curvature of the reflector at the normal incident point of the central ray. The hyperbolic traveltime can be derived by means of the paraxial ray theory ((Schleicher et al., 1993); (Tygel et al., 1997)) or by a geometrical approach (Höcht et al., 1999), and is given by

$$t^2_{CRS,hyp}(x_m,h) = (t_0 + \frac{2\sin\beta_0}{v_0}(x_m - x_0))^2 + \frac{2t_0\cos^2\beta_0}{v_0}(\frac{(x_m-x_0)^2}{R_N} + \frac{h^2}{R_{NIP}}). \quad (1)$$

As indicated above, $x_0$ and $t_0$ denote the emergence point of the normal ray on the seismic line and its ZO traveltime, respectively. The half-offset between source and receiver is denoted by $h$, whereas $x_m$ denotes the midpoint between source and receiver. The angle of emergence $\beta_0$ of the normal incidence ray, the radius of curvature $R_{NIP}$ and the radius of curvature $R_N$ are referred as CRS stacking attributes. The only required model parameter is the near-surface velocity $v_0$, and it is assumed to be known and constant in the vicinity of $x_0$.

**Special cases of CRS traveltime approximation**

An important stacking traveltime approximation can be obtained considering a diffraction situation or a diffracted central ray. In this case, the reflector segment collapses into a diffractor point, then the NIP and N waves are identical, i. e., $R_N = R_{NIP}$. Therefore, applying the latter identity, called diffraction condition, to equation (1) it reads

$$t^2_{CDS,hyp}(x_m,h)|_{R_N=R_{NIP}} = (t_0 + \frac{2\sin\beta_0}{v_0}(x_m - x_0))^2 + \frac{2t_0\cos^2\beta_0}{v_0}(\frac{(x_m-x_0)^2+h^2}{R_{NIP}}). \quad (2)$$

This new simplified traveltime approximation defines a new stacking surface called Common-Diffraction-Surface (CDS) and only depends on two attributes, $\beta_0$ and $R_{NIP}$. The stacking curves defined by (2) are approximations of the pre-stack Kirchhoff migration operator in the vicinity of each $P_0(x_0,t_0)$ on the referred operator. On the other hand, when it is considered the intersection of the 2-D CRS stacking surface with the plane $(x_m = x_0)$ of the common-midpoint (CMP) gather, we easily verify that equation (1) simplifies to the well-known CMP hyperbola (Hubral (1983))

$$t^2_{CMP,hyp}(x_m = x_0,h) = t_0^2 + \frac{2t_0\cos^2\beta_0}{v_0\,R_{NIP}}\,h^2. \quad (3)$$

A comparison of this equation with the well-known CMP stack formula

$$t^2_{CMP}(h) = t_0^2 + \frac{4}{v^2_{stack}}\,h^2, \quad (4)$$

reveals that the CRS traveltime reduces to the classic formula for this configuration. The stacking velocity $v_{stack}$ can now be expressed in terms of the CRS attributes:

$$v^2_{stack} = \frac{2v_0R_{NIP}}{t_0\cos^2\beta_0} \quad (5)$$

Now, the CMP traveltime approximation (3) only depends on one independent parameter,$v_{stack}$. Another special case results of the intersection of the CRS stacking surface with the plane of the ZO section $(h = 0)$. Then equation (1) is reduced to the following hiperbolic formula

$$t^2_{ZO,hyp}(x_m,h=0) = (t_0 + \frac{2\sin\beta_0}{v_0}(x_m - x_0))^2 + \frac{2t_0\cos^2\beta_0}{v_0R_N}(x_m-x_0)^2, \quad (6)$$

which depends of two CRS attributes $\beta_0$ and $R_N$. In a first-order approximation it is assumed that $R_N \to \infty$ implies plane normal waves emerging at the surface in $x_0$. In this consideration, equation (5) is reduced to the linear formula

$$t_{ZO,linear}(x_m,h=0)|_{R_N\to\infty} = t_0 + \frac{2\sin\beta_0}{v_0}(x_m - x_0). \quad (7)$$

This linear approximation only depends on one CRS attribute $\beta_0$. In the last special case it is assumed that a common-source or common-receiver point coincides with the central point $x_0$, which implies that the midpoint displacement $(x_m - x_0)$ equals to the half-offset $(h)$ in the common-shot/ common-receiver (CS/CR) gather, i. e., $(xm - x0) = h$, and equation (1) is again simplified to a hiperbola

$$t^2_{CS/CR,hyp}(x_m, h) = (t_0 + \frac{2\sin\beta_0}{v_0}(x_m - x_0))^2 + \frac{2t_0\cos^2\beta_0 h^2}{v_0}(\frac{1}{R_C}), \tag{8}$$

where

$$\frac{1}{R_C} = \frac{1}{R_N} + \frac{1}{R_{NIP}}, \tag{9}$$

Then the equation (8) depends only on the combined curvature $R_C$ and CRS attribute $\beta_0$. An important aspect of the general CRS stack traveltime approximation (1) is that it can be reduced to different mathematical expressions for specific applications, and this depends of the chosen data configuration (e.g. common-shot (CS), common-offset (CO), zero-offset (ZO), common-receiver (CR), common-midpoint (CMP)).

## CRS STACK AND CRS PARAMETERS SEARCH STRATEGIES

The CRS stack method simulates a ZO section from multi-coverage data by summing seismic events along the stacking surfaces corresponding to each sampling point $P_0(x_0, t_0)$ of the ZO section to be simulated. The stacking surface defined by (1) in the $(x_m, h, t)$ coordinates is based on three wavefront attributes $(\beta_0, R_{NIP}, R_N)$, referred to as the CRS stacking parameters. In the CRS stack method, for each ZO point, the three optimal attributes that define a stacking surface and that fits best to actual seismic events in the multi-coverage data, can be determined by means of automatic search processes based on coherency measure, evaluated along the several trials stacking surfaces, where the parameter triplet $(\beta_0, R_{NIP}, R_N)$ that produces the maximum coherency value is selected. The determination of the CRS stacking parameters is a typical optimization problem, which can be solved by applying a multidimensional global optimization algorithm that uses as objective function the coherency measure semblance, that depends upon the three independent parameters $\beta_0$, $R_{NIP}$ and $R_N$. The objective function of CRS stacking method is multimodal, i.e., a function with more than one local extremum. In general, the determination of global extremum and the corresponding optimal CRS parameter triplet, by applying a multidimensional global optimization algorithm, is computationally very expensive. To overcome this problem, the CRS stacking parameters can be searched-for by applying several strategies based on automatic search processes, but using the particular cases of the general hyperbolic approximation (1). Thus, in the next sections we concisely describe the two CRS parameters search strategies: The extended CRS search strategy and the global CRS search strategy. To simulate properly ZO sections with conflicting dip events, in addition to the global extremum it is necessary to consider at least one local extremum. Then, to simulate properly the interference of conflicting dip events, the extended CRS search strategy can consider more than one local extremum, and the global CRS search strategy consider only one local extrema. In the initial steps, for both strategies, the initial parameter triplet $(\beta_0^0, R_{NIP}^0, R_N^0)$ are determined, which are located close enough to the global extremum. These initial parameters triplet are used as initial approximations in the final three-dimensional local optimization step.

### Extended CRS search strategy

To split the three-parametric global optimization problem into separate one-parametric searches, the multi-coverage input data need to be sorted to specific gathers, such as CMP gather, CS/CR gather. The one-parametric searches in those families and in the ZO stacked section yields the initial attributes that can be used as first guess in a final local optimization step performed in whole pre-stack data. In this work the extended CRS search strategy is presented as being composed by four steps.

**STEP I : Automatic CMP stack.** This step is called *automatic CMP stack* due to its similarity to the familiar CMP stack method. The first one-parametric search is achieved in the CMP gathers using equation (3) to define the stacking curves. The coherency measure is evaluated along this stacking

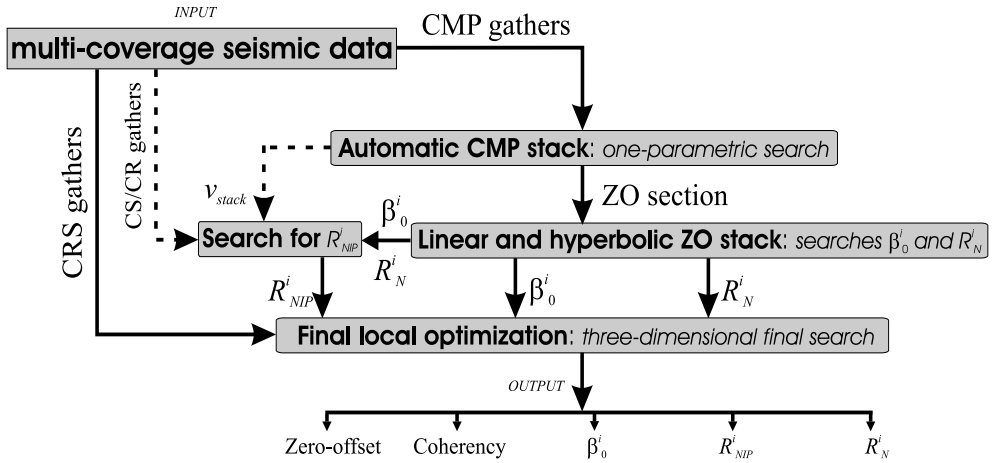


**Figure 1:** Flow chart of the CRS implementation based on extended search strategy. The index $i$ denotes the number of events that contributing each ZO sample.

curve, which depends on only one parameter called stacking velocity ($v_{stack}$), expressed by equation (5). To determine $v_{stack}$ yielding the highest coherence along the corresponding stacking curve, the coherency values are calculated along several stacking curves, then it is selected one which provides the highest coherency value. In this step, conflicting dips situations are not considered because the different contributing events may have very similar moveouts in the CMP gather. As main results, from this automatic CMP stack are obtained three sections: 1) coherency section, 2) $v_{stack}$ section and 3) simulated ZO section.

**STEP II : Linear and hyperbolic ZO searches.** In this step, the one-parametric linear ZO search is restricted to the simulated ZO section resulting from the automatic CMP stack, where the coherency measure is performed along the stacking curves given by (7). To solve the conflicting dip problem, the searches for additional emergence angles $\beta^i_0$ is performed, by generating an angle spectrum on a regular angle grid, namely, the coherence as function of the emergence angle. These spectra are analyzed according to the coherence maximum of events. The index *i* refers to the number of conflicting events. The determination of $R^i_N$, related to each $\beta^i_0$, is also performed in the CMP stacked section, but in this *hyperbolic ZO search* it is used the second-order approximation (6). The linear and the hyperbolic ZO searches are applied on the simulated ZO section obtained from the automatic CMP stack, and each of the one-parameter searches is applied on an initial grid of the respective parameter. As main results from this step, it results: 1)$\beta^i_0$ sections and 2)$R^i_N$ sections.

**STEP III : Hyperbolic CS/CR search.** In this stage of the searches, the $v_{stack}$ and the $\beta^1_0$ are available and with the help of equation (5) $R_{NIP}$ is calculated. The $v_{stack}$ is not significant in conflicting dip situations, therefore $R_{NIP}$ also is not significant. In these situations, it is required an additional search for $R^i_{NIP}$, which is performed on the CS/CR gather. With the knowledge of $\beta^i_0$, $R^i_N$ ,and $v_{stack}$, the range of possible values for the new radius of curvature $R_C$ can be well defined. The search for this parameter is similar to the search for $R^i_N$ , however, it is used the second-order approximation (8). Then, with equation (8) and the acquaintances it is determined $R^i_{NIP}$. As main output from this step, we have $R^i_{NIP}$ sections.

**STEP IV : Three-parametric local optimization.** In the final step it is used the traveltime approximation (1) for the local search process and this is performed in the pre-stack multicoverage data, where the attributes ($\beta^{0i}_0, R^{0i}_{NIP}, R^{0i}_N$), determined in the previous steps, are used as initial approximations for the local optimization using the *flexible polyhedron* algorithm. As final results obtained from the tree dimensional local optimization the following five optimized sections are obtained: 1) coherency section, 2) $\beta^i_0$ sections, 3) $R^i_{NIP}$ sections, 4) $R^i_N$ sections, and 5) simulated ZO section.

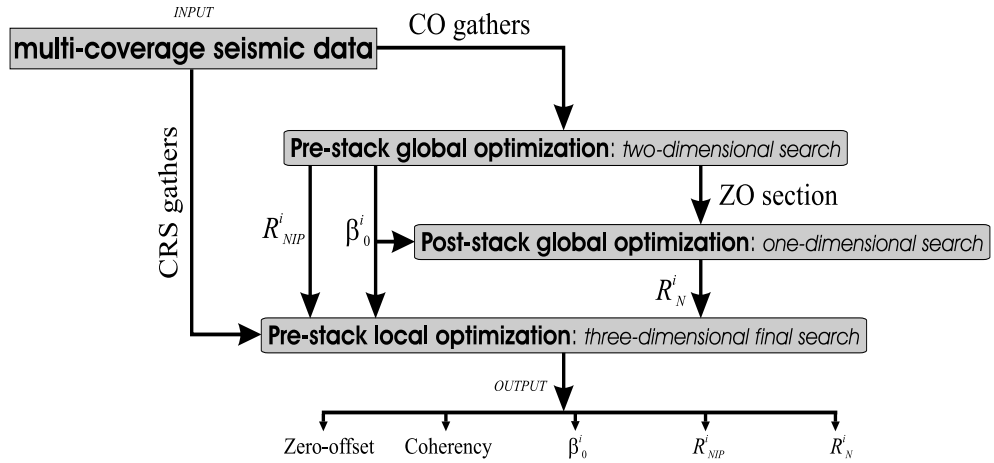


**Figure 2:** Flow chart describing the CRS stack implementation based on global search strategy. The index $i = 1, 2$ denotes the events detected for each ZO sample.

The procedure of application of the CRS stack based on extended CRS search strategy is described by the flow chart showed in Figure 1.

**Global CRS search strategy**

This strategy is based on global and local optimizations processes to search the three CRS parameters. The searches are performed in the pre-stack data and only the ZO section is used to perform one-parametric search.

**STEP I : Pre-stack global optimization.** In this step the parameters $\beta_0^i$ and $R_{NIP}^i$ are determined by means of two-parametric global search using the *Simulated Annealing* algorithm. The optimization process is performed in the pre-stack data using as an objective function the coherency semblance along the stacking surface, defined by equation (2). To take into account the conflicting dip events during the optimizations process the parameters associated to one local minimum are saved. The main results from this step are: 1) coherency section, 2) $\beta_0^i$ sections, 3) $R_{NIP}^i$ 4) simulated ZO section. The index $i = 1, 2$ refers to the global maximum and local maxima.

**STEP II : Post-stack global optimization.** This step uses the simulated ZO section from the first step to perform the one dimensional global search for parameter $R_N^i$. Again it is used the *Simulated Annealing* algorithm and the coherency measure is performed along the hyperbolic curves defined by equation (6). After repeating this procedure for all points $P_0$ of the ZO section to be simulated, as a main result it is obtained two $R_N^i$ sections.

**STEP III : Pre-stack global optimization.** In this final step it is used the local optimization *Quasi-Newton* algorithm to perform a local search for the best CRS parameters, using the previously estimated parameters ($\beta_0^{0i}, R_{NIP}^{0i}, R_N^{0i}$) as initial approximations. The optimization process is performed in pre-stack data and the traveltime approximation (1) is used to define the stacking surface along which it is performed the coherency measure. The final optimized results are: 1) coherency section 2) two $\beta_0^i$ sections; 3) two $R_{NIP}^i$ sections; 3) two $R_N^i$ sections and 4) simulated ZO section.

The flow chart with the processing steps of the CRS stack based on the global search strategy is showed in Figure 2.

## APPLICATIONS TO MARMOUSI DATA SET

In order to make the comparison of both CRS implementations it was decided to apply them to the complex synthetic 2-D Marmousi data set. A complete description of the well-known acoustic model and data

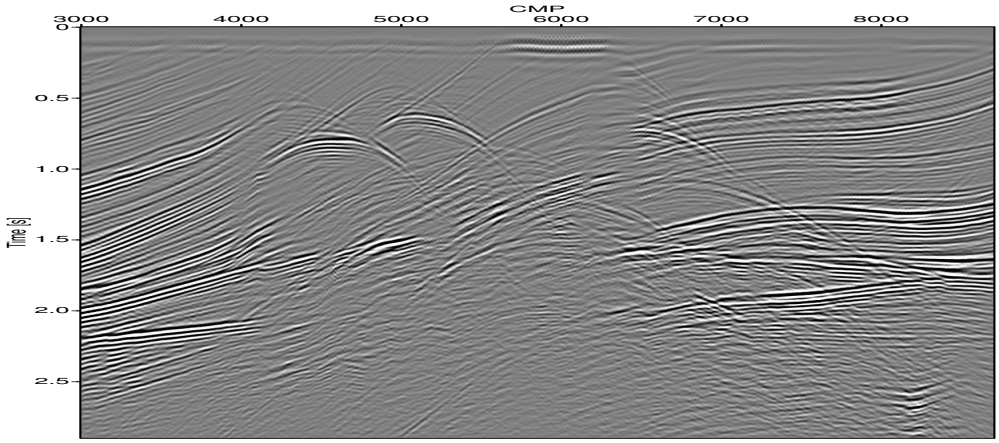


**Figure 3:** Simulated ZO section by the NMO/DMO stack method

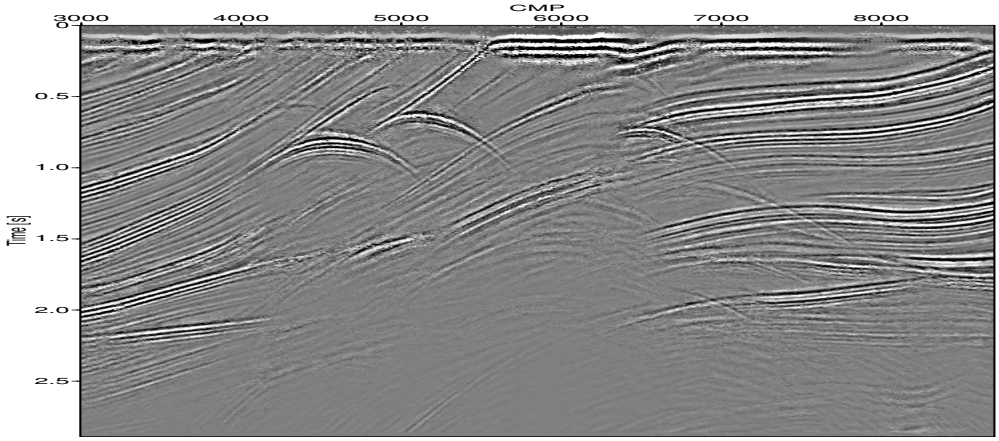


**Figure 4:** Simulated ZO section by the CRS stack based on extended search strategy

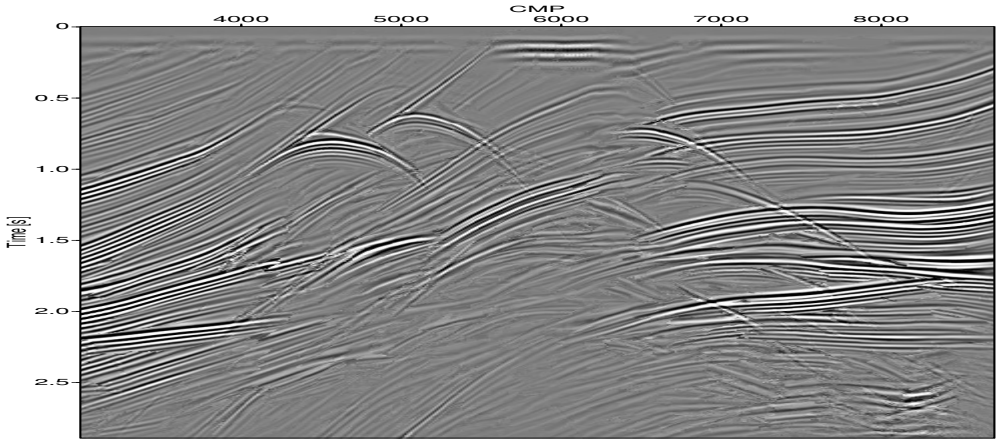


**Figure 5:** Simulated ZO section by the CRS stack based on global search strategy

acquisition can be found in Versteeg and Grau, (1991). Also for comparison, we include the ZO stacked section obtained by the conventional NMO/DMO stacking method (Figure 3), which was processed with the commercial seismic processing software FOCUS. It was used the Version 4.6 of the CRS stack implementation based on extended search strategy and in the CRS implementation based on global search strategy it was used the last version. For both CRS stack implementations, the input data was not submitted to any pre-processing phase. Also, it was not applied any kind of normalization to the input data. The processing parameters such as the aperture in the midpoint and offset coordinates were similar for boot CRS implementations. In the extended CRS search strategy was considered two conflicting events.

In Figure 4 we show the ZO stacked section obtained by the CRS stack, based on extended search strategy, and in Figure 5 the result of the CRS stack based on global search strategy. We show that the last CRS stack implementation provides a better image of the ZO section, mainly, in the deeper zones and in the complex central zone of the Marmousi model, when compared with their counterparts in the first CRS section and in the NMO/DMO section. The global CRS search strategy implementation was able to image events that can not seen in the other CRS result and in the result obtained by the NMO/DMO stack. The Figure 6 shows the coherence section, the emergence angle section, the radius of curvature of the NIP wave section and the radius of curvature of the N wave section, which were obtained from the first CRS stack implementation. In a similar way, in the Figure 7 are showed the coherency section and the tree attributes sections obtained by the CRS stack based on global optimization strategy. We see that CRS attributes are better estimated by the last CRS stack strategy, being this fact important for the subsequent application of these attributes.

## CONCLUSIONS

Both CRS strategies are evaluated in the Marmousi data set, demonstrating the CPU efficiency and accuracy of both approaches. The application reveals that the extende search strategy is more efficient in terms of CPU time (approximately tree times) compared to the global search strategy. On the other hand, the CRS stack based on global search strategy significantly improves the image quality in the complex zone of the Marmousi model, when compared to the results of first CRS stack implementation, as well as to the conventional NMO/DMO staking method. This fact indicates that the CRS stack based on global search estrategy can provide good improvements to the post-stack time- or depth-migrated images of tectonically complex areas. Furthermore, the CRS attributes estimated by the last CRS implementation are better estimated than those obtained by the first CRS implementation.

## ACKNOWLEDGMENTS

The second author thanks the National Petroleum Agency (ANP-Brazil) for scholarships during his master studies at the Federal University of Pará, Brazil. This work was kindly supported by the sponsors of the *Wave Inversion Technology (WIT) Consortium*, Karlsruhe, Germany.

## REFERENCES

Bergler, S., Marchetti, P. H. P., Cristini, A., and Cardone, G. (2002). 3d common-reflection-surface stack and kinematic wavefield attributes. *The Leading Edge*, 21(10):1010–1015.

Biloti, R., Santos, L., and Tygel, M. (2002). Multiparametric traveltime inversion. *Studia Geophysica et Geodetica*, 46:177–192.

Birgin, E. G., Biloti, R., Tygel, M., and Santos, L. (1999). Restricted optimization: a clue to a fast and accurate implementation of the common reflection surface stack method. *Journal of Applied Geophysics*, 42:143–155.

Duveneck, E. (2004). Velocity model estimation with data-derived wavefront attributes. *Geophysics*, 69:265–274.

Garabito, G., Cruz, J. C., Eiras, J., and Queiroz, N. P. (2003). Application of the crs stack to seismic data of amazon paleozoic basin. *8th. International Congress of Brazilian Geophysical Society, Expanded Abstracts. Rio de Janeiro, Brazil.*

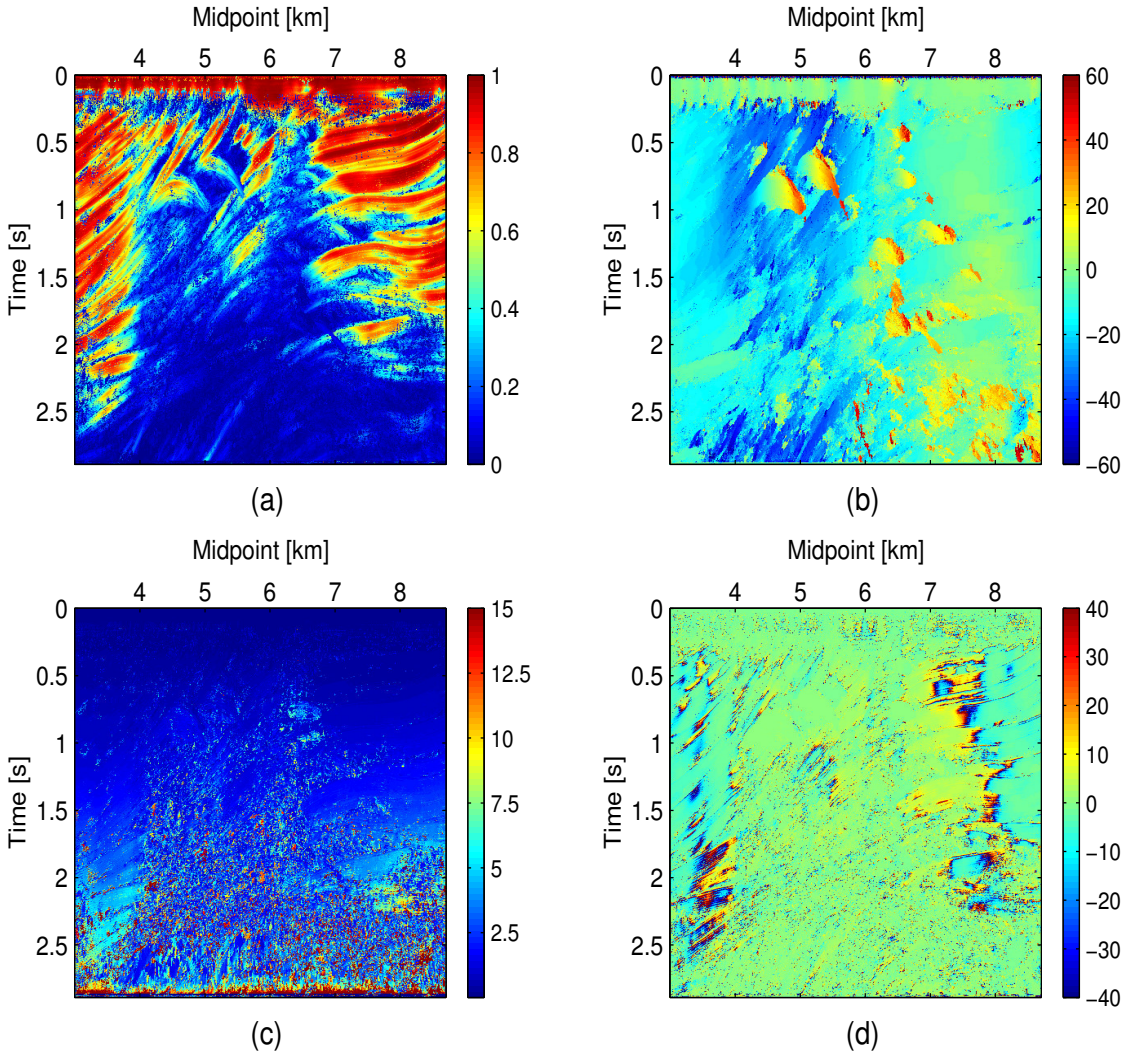


**Figure 6:** CRS attributes obtained by extended search strategy: a) Coherency, b) Emergence angle [deg.], c) Radius of NIP wavefront [km], d) Radius of N wavefront [km].

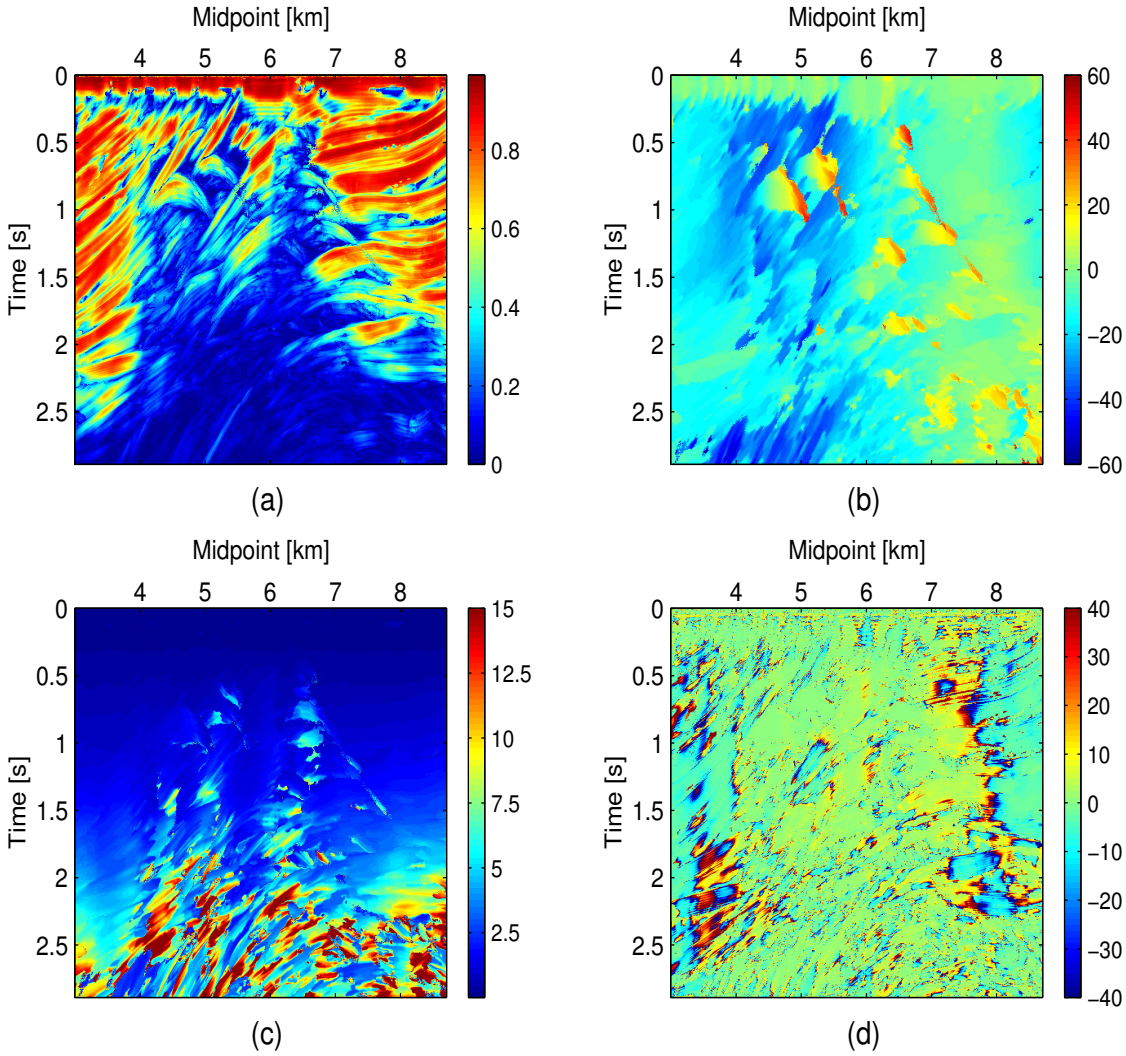


**Figure 7:** CRS attributes obtained by global search strategy: a) Coherency, b) Emergence angle [deg.], c) Radius of NIP wavefront [km], d) Radius of N wavefront [km].

Garabito, G., Cruz, J. C., Hubral, P., and Costa, J. (2001). Common reflection surface stack: A new parameter search strategy by global optimization. *71th. SEG Mtg., Expanded Abstracts. San Antoinio, Texas,USA*.

Gierse, G., Preuessmann, J., Laggiard, E., Boeennemann, C., and Meyer, H. (2003). Improved imaging of 3d marine seismic data from offshore costa rica by crs processing. *First Break*, pages 45–49.

Gill, P. E., Murray, W., and Wright, M. H. (1981). *Practical Optimization*. Academic Press, London and New York.

Höcht, G., de Bazelaire, E., Majer, P., and Hubral, P. (1999). Seismic and optics: Hyperbolae and curvatures. *J. Appl. Geophys.*, 42(3):261–281.

Hubral, P. (1983). Computing true amplitude reflections in a laterally inhomogeneous earth. *Geophysics*, 48:1051–1062.

Hubral, P. (1999). Special issue: Macro-model independent seismic reflection imaging. *Journal of Applied Geophysics*, 42(3).

Jäger, R., Mann, J., Höcht, G., and Hubral, P. (2001). Common reflection surface stack: Image and attributes. *Geophysics*, 66:97–109.

Kirkpatrick, S., Gelatt, C., and Vecchi, M. (1983). Optimization by simulated annealing. *Science*, 220:671–680.

Mann, J. (2001). Common-reflection-surface stack and conflicting dips. *In Extended Abstracs, 71th Annual Internat. Mtg., Expl. Geophys*.

Mann, J., Jäger, R., Müller, T., Höcht, G., and Hubral, P. (1999). Common-reflection-surface stack - a real data example. *Journal of Applied Geophysics*, 42:301–318.

Müller, T. (1998). Common reflection surface stack versus nmo/stack and nmo/dmo/stack. *60th Mtg. Eur.Assoc. Expl. Gophys., Extended Abstracts*.

Nelder, J. A. and Mead, R. (1965). A simplex method for function minimization. *Computer Jornal*, 7.

Pruessmann, J., Coman, R., Enders, H., and Trappe, H. (2004). Improved imaging and avo analysis of a shallow gas reservoir by crs. *The Leading Edge*, 23(9):915–918.

Schleicher, J., Tygel, M., and Hubral, P. (1993). Parabolic and hyperbolic paraxial two-point traveltimes in 3d media. *Geophys. Prosp.*, 41:495–513.

Trappe, H., Gierse, G., and Pruessmann, J. (2001). Case studies show potential of common reflection surface stack - structural resolution in the time domain beyond the conventional NMO/DMO stack. *First Break*, 19:625–633.

Tygel, M., Müller, T., Hubral, P., and Schleicher, J. (1997). Eigenwave based multiparameter traveltime expansions. *Expanded Abstract of the 67th Annual Internat. Mtg., Soc. Expl. Geophys*.